Modelling DAS signals for hydraulic fracturing and caprock monitoring

Matt Eaid and Kris Innanen

ABSTRACT

Passive seismic technologies are indispensable tools for monitoring hydraulic fracture growth, caprock integrity during cyclic steam stimulation (CSS) and CO2 sequestration, and borehole casing integrity. Mature fields use a combination of permanent arrays and temporary wireline tools to monitor the reservoir and optimize production. Conventionally, passive seismic monitoring consists of large arrays of surface and downhole geophones. This can result in the drilling of dedicated monitor wells, and well shut-in during wireline monitoring, resulting in elevated costs. Distributed acoustic sensing (DAS) uses non-invasive optical fibres that can be cemented behind casing in producing and injecting wells, offering an opportunity for the dual purposing of wells and reduced monitoring costs. DAS has the potential to be a powerful reservoir monitoring technology. To better understand the capabilities of DAS for reservoir monitoring, we develop an analytic modeling tool for DAS signals from moment tensor sources, providing data like that expected from hydraulic fracturing and CSS treatments. This tool provides an efficient means of examining DAS signals from various moment tensor sources. In this paper this tool is used to investigate the diagnostic characteristics in the DAS signals from different moment tensor sources and gain an enhanced understanding of the effect of source mechanics on DAS signals.

INTRODUCTION

The capabilities of distributed acoustic sensing (DAS) has grown significantly in recent years. Early studies tended to focus on the use of distributed acoustic sensors as an alternative to geophones in vertical seismic profiles (Mestayer et al., 2012; Mateeva et al., 2014). However in recent years, DAS has found applications in smart-cities using passive seismic for traffic pattern analysis (Dou et al., 2017; Cova et al., 2018), full waveform inversion (Podgornova et al., 2017; Eaid et al., 2019), and infrastructure integrity. DAS has also carved out a niche in reservoir monitoring capabilities of mature fields during hydraulic fracturing and cyclic steam stimulation (CSS), offering opportunities for real time optimization of treatment schedules for optimal fracture growth and real time assessment of caprock integrity. Employing non-invasive optical fibre, DAS can be placed in abandoned wells, directly in producing wells, or in wells during fracturing treatments. The dual purposing of wells negates the need for dedicated monitor wells, reducing cost, a feat not always achievable with geophones. Recent studies have investigated the use of DAS for microseismic monitoring during hydraulic fracturing (Jin and Roy, 2017; Becker et al., 2018; Karrenbach and Cole, 2019).

Many of these studies have focused on the interpretation of field data to gain insights into fracture treatment. However, it is also important to develop strategies for modeling DAS signals from passive moment tensor type sources both to better understand field data, but also to develop strategies for event localization and moment tensor inversions of DAS

data. Accurate modeling of shot records will provides insights into features in the data associated with rock failure allowing for enhanced monitoring of reservoir conditions during hydraulic fracture treatments and CSS. Eaid et al. (2018) developed methods for modeling the response of shaped DAS fibres to moments tensor sources from microseismic events. That study focused on finite difference type approaches to generating DAS shot records from moment tensor sources, providing detailed modeling of DAS data. In this study we develop an analytic modeling tool for DAS data from moment tensor sources. While this tool does not provide as much detail as finite difference type methods, it provides an efficient means of analyzing DAS data from many moment tensor sources. Significant information about hydraulic fracture treatments are contained in the direct arrivals, and the method developed here allows for rapid investigation of the effect of source mechanics on these direct arrivals, and allows for enhanced design of reservoir monitoring arrays.

FORCE COUPLES AND MICROSEISMIC SOURCES

Natural faulting, in which rocks fail causing displacement across a plane, is a source of significant seismic energy resulting in many earthquakes annually. Anthropogenic activity can alter the subsurface stress field resulting in failure on existing faults or the creation of new faults. This rock failure can be intentional to engineer permeability as in hydraulic fracture treatments, or an unintentional consequence during cyclic steam stimulation where caprock integrity is compromised. Typically, anthropogenic seismicity results in small earthquakes below a magnitude of zero, and is termed microseismicity. Regardless of the source, or intention of anthropogenic microseismicity, it is important to develop modeling strategies with the ultimate goal of enhancing our understanding of the underlying mechanisms leading to the seismicity.

When modeling exploration seismic data an explosive or vertically directed point source is typically assumed, depending on if we are interested in dynamite or Vibroseis type sources. The seismic waves generated by the failure of rock are typically more complicated. Intuitively, earthquakes, which are a result of slip on a fault plane, where theorized to originate from pair of forces acting in opposite directions separated by a small distance across the fault plane. However, this interpretation is problematic, a force couple of this type induces a torque not evident in shear faults in the field. To compensate for this, an orthogonal force couple acting on an auxiliary plane was theorized, and later proven by Maruyama (1963). While this model, known as the double couple, fit most earthquakes well, it failed in regions of volcanic and geothermal activity where seismic sources can be related to volumetric changes. To incorporate earthquakes of this type, we must turn to moment tensor type sources.

From elementary physics a torque or moment due to a force couple is equal to the magnitude of the applied forces multiplied by the perpendicular distance between them. Assuming earthquakes are generated by force couples separated by some distance, then this idea can be extended to seismic sources caused by rock failure. Figure 1 shows a force couple of magnitude f separated by a small distance ξ_k.

The moment generated by these forces is given by,

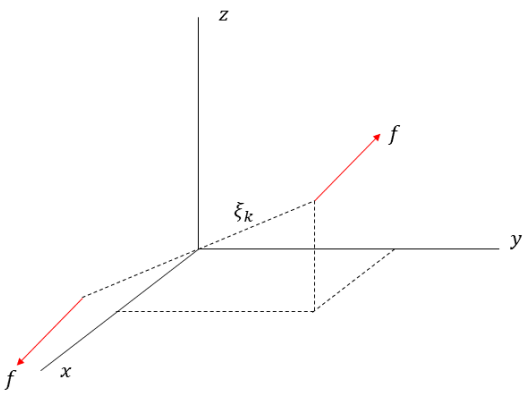

FIG. 1. Schematic representaion of a force couple of magnitude f separeted by distance ξ_k acting across a fault plane.

$$\mathbf{M} = \mathbf{f}\xi_k \tag{1}$$

with the definitions of $\mathbf{f}$ and ξ_k given above. This concept can be expanded into a rank 2 moment tensor, the components of which are given by,

$$M_{ij} = \int\int\int_V f_i(\xi)\xi_j d^3\xi \tag{2}$$

where the moment is now integrated over the entire source region. This can be further written in tensor notation as,

$$M_{ij} = \begin{bmatrix} M_{11} & M_{12} & M_{13} \\ M_{21} & M_{22} & M_{23} \\ M_{31} & M_{32} & M_{33} \end{bmatrix}. \tag{3}$$

Each component of the tensor in equation 3 represents a force couple acting in the i^{th} direction separated by a distance ξ in the j^{th} direction. The moment tensor is symmetric so that in the case of double couples no net torque is induced. Off diagonal components describe shear slip, while the diagonal components describe volumetric changes in the volume effected by the source. A positive trace indicates volumetric expansion, a negative trace volumetric compression, and a trace of zero indicates no net volume change.

Moment tensors are commonly decomposed into three basic types of sources (Knopoff and Randall, 1970), each of which has a clear physical interpretation,

$$\mathbf{M} = \mathbf{M}_{ISO} + \mathbf{M}_{DC} + \mathbf{M}_{CLVD}. \tag{4}$$

The isotropic component $\mathbf{M}_{ISO}$ describes sources resulting in volume changes in the medium, and encompasses explosive sources such as dynamite and tensile cracks opening due to fluid injection. The second term, $\mathbf{M}_{DC}$ describes the double couple components described above. The final term, $\mathbf{M}_{CLVD}$ describes compensated linear vector dipole type sources associated with a tensile crack opening compensated by slip on two orthogonal planes, so that no net volume change occurs. These four source types will be investigated for their effect on microseismic DAS data.

ANALYTIC DISPLACEMENT FROM A FORCE COUPLE

The direct arrivals from microseismic sources, containing p-wave and s-wave energy, reveal important characteristics about their sources, including location and the mechanism for rock failure. These direct arrivals are commonly used in microseismic analysis during hydraulic fracture and CSS treatments. While lacking information about scattered waves, analytic solutions to the wave equation provide an efficient means for gaining insight into the behavior of these direct arrivals. Aki and Richards (1980) develop analytic solutions to the elastic wave equation for moment tensor type sources that allow for the computation of the displacement u_i at a distance r for moment tensor source M_{jk},

$$
\begin{aligned}
u_i = & \left(\frac{15\gamma_i\gamma_j\gamma_k - 3\gamma_i\delta_{jk} - 3\gamma_j\delta_{ik} - 3\gamma_k\delta_{ij}}{4\pi\rho} \right) \frac{1}{r^4} \int_{r/\alpha}^{r/\beta} \tau M_{jk} s(t-\tau) d\tau \\
& + \left(\frac{6\gamma_i\gamma_j\gamma_k - \gamma_i\delta_{jk} - \gamma_j\delta_{ik} - \gamma_k\delta_{ij}}{4\pi\rho\alpha^2} \right) \frac{1}{r^2} M_{jk} s\left(t - \frac{r}{\alpha}\right) \\
& - \left(\frac{6\gamma_i\gamma_j\gamma_k - \gamma_i\delta_{jk} - \gamma_j\delta_{ik} - 2\gamma_k\delta_{ij}}{4\pi\rho\beta^2} \right) \frac{1}{r^2} M_{jk} s\left(t - \frac{r}{\beta}\right) \\
& + \frac{\gamma_i\gamma_j\gamma_k}{4\pi\rho\alpha^3} \frac{1}{r} M_{jk} \dot{s}\left(t - \frac{r}{\alpha}\right) - \left(\frac{\gamma_i\gamma_j - \delta_{ij}}{4\pi\rho\beta^3} \right) \gamma_k \frac{1}{r} M_{jk} \dot{s}\left(t - \frac{r}{\beta}\right)
\end{aligned} \tag{5}
$$

where, $\gamma_n = x_n/r$ is the directional cosine between the source and a point on the wavefield, $s(t)$ is the time dependent source function, $\dot{s}(t)$ is its time derivative, α is the p-wave velocity and β is the s-wave velocity. The expression for the displacement consists of a near field component with $r^{-4} \int_{r/\alpha}^{r/\beta} \tau M_{jk} s(t-\tau) d\tau$ dependence, two intermediate field terms with r^{-2} dependence, and two far field terms with r^{-1} dependence. The near field terms dominate at small distances close to the source, typically within one wavelength, while at distances much greater than a wavelength the far field terms dominate. The far field term can be seen to consist of the superposition of a wave traveling with speed α, and a wave traveling with speed β. These terms represent the analytic expressions for p-wave and s-wave first arrivals seen on geohpone seismograms. The leading terms of each expression coupled with the moment tensor represent what is known as the radiation pattern and control the angular dependence on the radiated seismic energy. These radiation patterns are important fro understanding how seismic radiates away from a given source type.

STRAIN RESPONSE OF DISTRIBUTED ACOUSTIC SENSORS

Distributed acoustic sensing uses optical fibres to sense the strain due to propagating seismic wavefields (Masoudi et al., 2013). Due to the rigidity of the glass in the optical fibres, DAS suffers from broadside insensitivity and is only sensitive to components of the wavefield inducing tangential strain in the fibre. Modeling of DAS data generally begins with the development of a geometric model whose main goal is the computation of an orthonormal basis containing the fibre tangent **t** at every point along the fibre, as well as the normal **n** and binormal **b** to the tangent (Innanen, 2017; Eaid et al., 2018). The next step is the computation of the strain field from the standard definition of the strain tensor,

$$\epsilon_{\mathbf{c}} = \frac{\nabla_x \mathbf{u} + (\nabla_x \mathbf{u})^T}{2} \tag{6}$$

where ϵ_c is the strain tensor in Cartesian coordinates,

$$\epsilon_c = \begin{bmatrix} \epsilon_{xx} & \epsilon_{xy} & \epsilon_{xz} \\ \epsilon_{yx} & \epsilon_{yy} & \epsilon_{yz} \\ \epsilon_{zx} & \epsilon_{zy} & \epsilon_{zz} \end{bmatrix}. \tag{7}$$

To compute the response of a DAS fibre we require the strain field in the coordiante system of the fibre. This is achieved through the projection of the field orthonormal basis onto the fibre orthonormal basis, through the formula for the rotation of a rank 2 tensor,

$$\epsilon_f = \mathbf{R}\epsilon_c\mathbf{R}^{\mathrm{T}} \tag{8}$$

where $\epsilon_f = \epsilon(\mathbf{t}, \mathbf{n}, \mathbf{b})$ is the strain field in the coordinates of the fibre. The matrix **R** is the rotation matrix taking the strain from field to fibre coordinates,

$$\mathbf{R} = \begin{bmatrix} \hat{\mathbf{t}}\cdot\hat{\mathbf{1}} & \hat{\mathbf{t}}\cdot\hat{\mathbf{2}} & \hat{\mathbf{t}}\cdot\hat{\mathbf{3}} \\ \hat{\mathbf{n}}\cdot\hat{\mathbf{1}} & \hat{\mathbf{n}}\cdot\hat{\mathbf{2}} & \hat{\mathbf{n}}\cdot\hat{\mathbf{3}} \\ \hat{\mathbf{b}}\cdot\hat{\mathbf{1}} & \hat{\mathbf{b}}\cdot\hat{\mathbf{2}} & \hat{\mathbf{b}}\cdot\hat{\mathbf{3}} \end{bmatrix}. \tag{9}$$

The component in the upper left corner of ϵ_f is the tangential component of strain sensed by the fibre. Expanding equation (8) with the definition of **R** given by (9) and extracting the upper left term results in,

$$\epsilon_{tt} = (\hat{\mathbf{t}}\cdot\hat{\mathbf{1}})^2\epsilon_{xx} + 2(\hat{\mathbf{t}}\cdot\hat{\mathbf{1}})(\hat{\mathbf{t}}\cdot\hat{\mathbf{2}})\epsilon_{xy} + 2(\hat{\mathbf{t}}\cdot\hat{\mathbf{1}})(\hat{\mathbf{t}}\cdot\hat{\mathbf{3}})\epsilon_{xz} + (\hat{\mathbf{t}}\cdot\hat{\mathbf{2}})^2\epsilon_{yy} + (\hat{\mathbf{t}}\cdot\hat{\mathbf{2}})(\hat{\mathbf{t}}\cdot\hat{\mathbf{3}})\epsilon_{yz} + (\hat{\mathbf{t}}\cdot\hat{\mathbf{3}})^2\epsilon_{zz}. \tag{10}$$

Equation (10) is the expression for the strain sensed by a DAS fibre due to an impinging wave. The strain response is a weighted sum of the Cartesian strain components, where the weights represent the sensitivity of the fibre to each strain component and are geometry dependent.

ANALYTIC STRAIN FROM A FORCE COUPLE

To compute the analytic response of a DAS fibre to waves radiated by moment tensor type sources, we require analytic expressions for the strain produced by these sources. This can be achieved by applying the definition of the strain tensor in equation (6) to the analytic displacement in equation (5). We present a far field approximation here, both for simplicity and because the far field dominates at the distances in which microseismic signals are typically recorded. In deriving the analytic strain we make use of the following identities

$$\frac{\partial r}{\partial x_q} = \gamma_q \qquad \frac{\partial \gamma_i}{\partial x_q} = \frac{\delta_{iq} - \gamma_i \gamma_q}{r} \qquad \frac{\partial r^{-n}}{\partial x_q} = \frac{-n}{r^{n+1}} \gamma_q.$$

Computation of the far field strain terms requires derivatives of the intermediate and far field displacement terms with respect to x, keeping only terms with r^{-1} dependence. This results in,

$$\epsilon_{ij} = \epsilon_{ij}^{PF_f} + \epsilon_{ij}^{SF_f} \tag{11}$$

where $\epsilon_{ij}^{PF_f}$ is the p-wave component of the far field and $\epsilon_{ij}^{SF_f}$ is the s-wave component. Computing the derivatives with the above identities gives,

$$\epsilon_{ij}^{PF_f} = c_\alpha^F \left(\frac{m \gamma_i \gamma_j}{r} \right) \ddot{s}(t - r/\alpha) \tag{12}$$

$$\epsilon_{ij}^{SF_f} = c_\beta^F \left(\frac{m \gamma_i \gamma_j - \Gamma_{ij}}{r} \right) \ddot{s}(t - r/\alpha) \tag{13}$$

where,

$$m = \gamma_i M_{ij} \gamma_j \qquad \Gamma_{ij} = \frac{\gamma_i' \gamma_j + \gamma_i \gamma_j'}{2} \qquad \gamma_i' = \delta_{ip} M_{pq} \gamma_q$$

$$c_\alpha^F = -\frac{1}{4\pi\rho\alpha^4} \qquad c_\beta^F = \frac{1}{4\pi\rho\beta^4}$$

These expressions differ from the terms for the far field displacement from moment tensor sources. They both still decay with distance traveled (r^{-1}), but the radiation patterns now differ, and the wavefield is a function of the second time derivative of the source

function. The signals recorded by DAS are thus a 90 degree phase shift of those recorded by geophones. Additionally, strain is radiated in a different manner than displacement due to moment tensor type sources. Affecting the data differently at various angles. The fibre response due these far field strains is obtained through the weighted sum of the strain components using equation (10). The weights are dependent on the projection of the field coordinates onto the fibre coordinates and are therefore a function of the fibre geometry.

MICROSEISMIC EXAMPLES

The above analytic expressions in equations (12) and (13) for the far field strain due to moment tensor sources coupled with equation (10) provide a means of computing the response of a DAS fibre to microseismic type sources. We examine the effect of different source mechanisms on the seismic signal recorded by a DAS fibre with the goal of gaining insight into how the data is affected by the mechanism for rock failure. A straight DAS fibre is placed in a horizontal well with a landing depth of 9300 feet, the horizontal of the well is 5700 feet, and the vertical extends to a depth of 8800 feet. A microseismic source is initiated at location of $\vec{xs} = (2415, 300, 9200)$ feet from the wellhead. The geometry of this experiment is shown in figure 2.

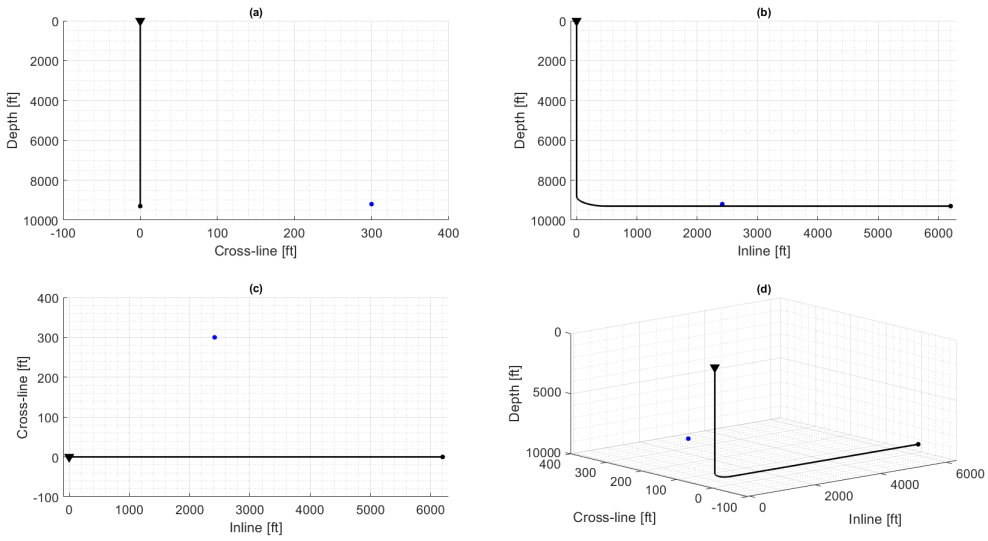

FIG. 2. Geometric design for modeling DAS seismic records from moment tensor sources. Barrel view (a), profile view (b), map view (c), volumteric view (d). The blue cirlce indicates the source location. The black line depicts the well trajectory containing the fibre where the triangle represents the wellhead and the black circle the well toe.

To gain insight into the effect of the source mechanism on the seismic data recorded by DAS, we compare records from explosive, double couple, tensile crack, and compensated linear vector dipole type sources. In this analysis we assume that the well is drilled on azimuth, meaning that the well azimuth is aligned with the minimum principal stress. Wells in hydraulic fracture stimulation are typically drilled on azimuth to allow for maximum fracture propagation perpendicular to the well bore. In this case fractures tend to open, or slip parallel to the minimum horizontal stress, or in the direction of the well bore. This study considers moment tensor sources associated with rock failure on planes parallel and perpendicular to the well bore. The moment tensors consider are shown below,

$$\mathbf{M}_{expl} = \begin{bmatrix} 1 & 0 & 0 \\ 0 & 1 & 0 \\ 0 & 0 & 1 \end{bmatrix} \qquad \mathbf{M}_{dc} = \begin{bmatrix} 0 & 1 & 0 \\ 1 & 0 & 0 \\ 0 & 0 & 0 \end{bmatrix}$$

$$\mathbf{M}_{clvd} = \begin{bmatrix} 1 & 0 & 0 \\ 0 & -2 & 0 \\ 0 & 0 & 1 \end{bmatrix} \qquad \mathbf{M}_{tc} = \begin{bmatrix} 2 & 0 & 0 \\ 0 & 1 & 0 \\ 0 & 0 & 1 \end{bmatrix}$$

where $\mathbf{M}_{expl}$ represents an explosive source, $\mathbf{M}_{dc}$ a double couple source characteristic of strike slip shear faulting, $\mathbf{M}_{clvd}$ a compensated linear vector dipole representative of a tensile crack closing in the y-direction, compensated by slip on two orthogonal planes, and $\mathbf{M}_{tc}$ is the moment tensor for a tensile crack opening in the x-direction due to fluid injection. These sources types were chosen for analysis due their association with anthropogenic activity such as tensile cracks opening during hydraulic fracture treatments. The explosive source, while not commonly encountered in microseismic surveys, provides an easy to understand benchmark for our analysis.

These moment tensor are used in equations (12) and (13) to compute the far-field p-wave and s-wave strain produced by different source mechanisms. The strain fields are then projected onto the fibre using equation (10), with the weights dependent on the fibre geometry. The horizontal portion of the fibre in figure 2 has a tangent oriented in the x-direction, assuming a straight fibre, it is therefore only sensitive to ϵ_{xx} components of strain. The vertical portion has a tangent in the z-direction and is only sensitive to ϵ_{zz}. Within the heel portion of the well, the tangent slowly turns from fully oriented in z, to fully oriented in x. Portions of the fibre in the heel have mixed sensitivity to ϵ_{xx} and ϵ_{zz} dependent on the fibre tangent direction.

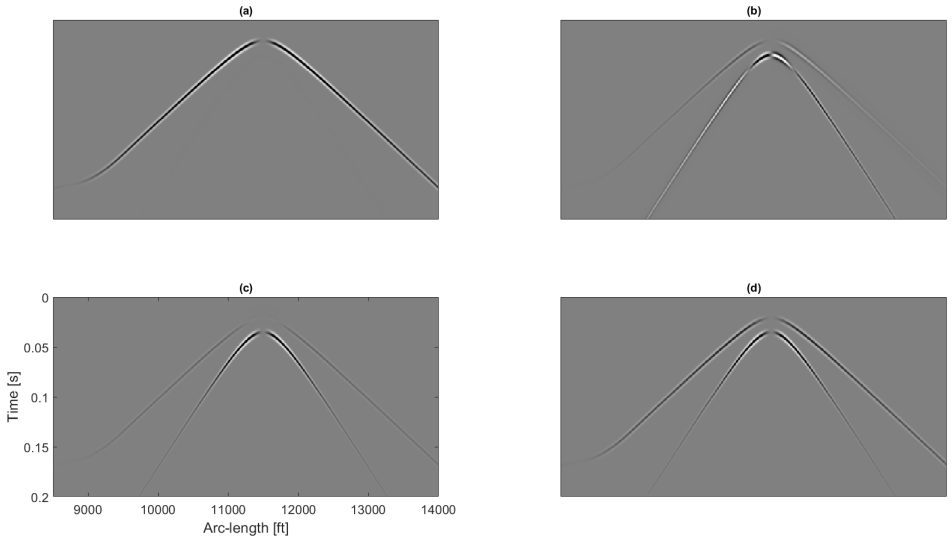

FIG. 3. Distributed acoustic sensing seismic records for (a) an explosive source, (b) double couple source, (c) CLVD source, (d) tensile crack opening source.

Figure 3 shows the seismic records recorded by a DAS fibre for an explosive source (a), double couple source (b), CLVD source (c), and a tensile crack source (d). These records reveal some important features of the data recorded by a fibre in a horizontal well. Importantly, fibres deployed in horizontal wells allow for the deployment of sensors close to the hypocenter of the seismic source allowing for increased sensitivity. Additionally, the long offsets provided by the horizontal fibre supply information from large solid angles of the radiated seismic energy, a crucial feature for successful inversion for the moment tensor. This manifests in the modeled data, as diagnostic features in the p-wave and s-wave arrivals from the varying source types.

The explosive source was used as a bench mark for the successful application of this algorithm. The p-wave energy is symmetric about the source position along the fibre, with a reduction in the sensitivity at near normal incidence angles, a phenomenon known as broadside insensitivity of DAS fibres (Kuvshinov, 2015). Additionally, the radiated energy from the explosive source lacks a shear arrival as expected. The seismic records from the other three sources also contain important diagnostic features. Starting with the double couple source, the record shows a strong S/P wave amplitude ratio. Another significant diagnostic feature is the distinct s-wave polarity pattern seen in the record from the double couple source, a feature not seen on the other records. Finally the p-wave flips polarity about the source position, another feature unseen on the other records. The diagnostic features differentiating the CLVD source in figure 3(c) and the tensile crack source in figure 3(d) are subtler. Tensile crack sources tend to have balanced S/P wave amplitude ratios of approximately 3, which is exemplified in the record of figure 3(d). Both tensile cracks and CLVD sources have symmetric p-wave and s-wave polarity patterns about the source position. A key diagnostic feature of CLVD sources is the polarity reversal towards zero offset, which tends to manifest as a wider dim zone due to the weak radiated energy. While this analysis is not a comprehensive study of all of the possible moment tensor sources, it highlights the key features diagnostic of certain moment tensor sources, and unlocks the potential for efficient understanding of the effect of different moment tensor sources on the data. While not shown here, it is important to note that this analysis was compared to field data with strong correlations, and the ability to infer moment tensor sources from forward modeling.

The features in the data discussed above can be understood by analysis of the radiation patterns for different sources. In equations (12) and (13) the terms in the numerator of the fractions in the parentheses describe the radiation patterns of the strain components for p-wave and s-wave energy respectively. These radiation patterns describe the angle dependent radiation of seismic energy away from the source and are a function of the moment tensor. Radiation patterns are diagnostic of particular source types and aid in identifying source mechanics. Figure 4 shows the p-wave radiation patterns for a double couple source with (a) ϵ_{xx}, (b) ϵ_{yy}, (c) ϵ_{zz}, (d) ϵ_{xy}, (e) ϵ_{xz}, (f) ϵ_{yz}, while figure 5 shows the same for the s-wave radiation pattern.

The horizontal portion of the fibre in figure 2 is only sensitive to the ϵ_{xx} component of strain. We can therefore understand the features in the data by looking at those components of the radiation patterns for the p-wave and s-wave. Figure 6 shows the ϵ_{xx} components of the p-wave (top row) and s-wave (bottom row) radiation patterns for an explosive source,

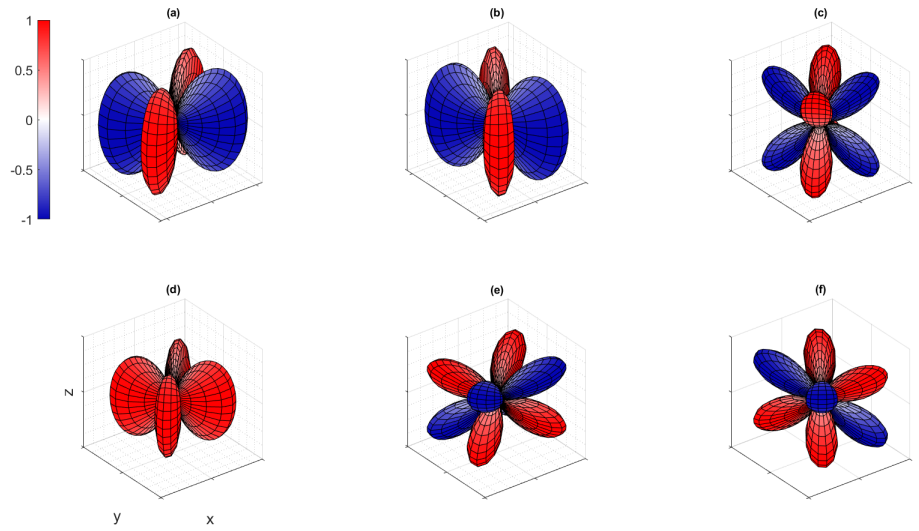

FIG. 4. P-wave radiation patterns for a double couple source, (a) ϵ_{xx}, (b) ϵ_{yy}, (c) ϵ_{zz}, (d) ϵ_{xy}, (e) ϵ_{xz}, (f) ϵ_{yz}

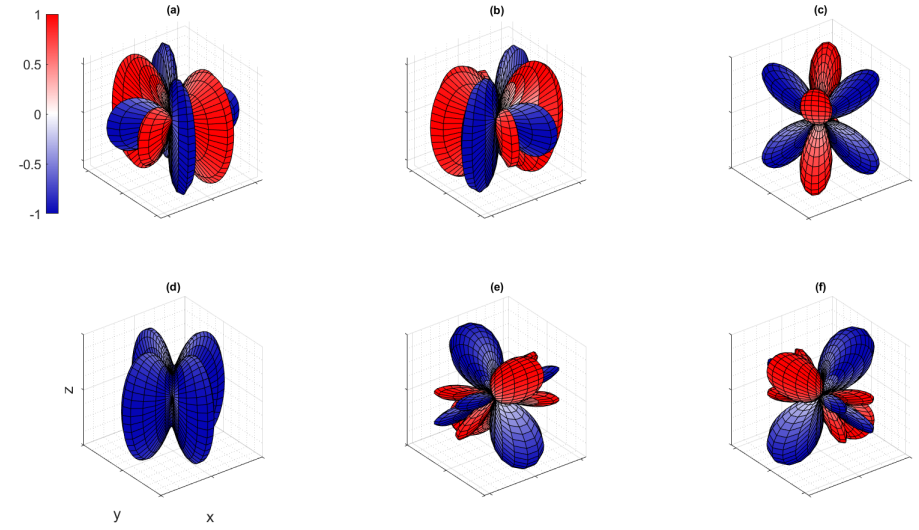

FIG. 5. S-wave radiation patterns for a double couple source, (a) ϵ_{xx}, (b) ϵ_{yy}, (c) ϵ_{zz}, (d) ϵ_{xy}, (e) ϵ_{xz}, (f) ϵ_{yz}

double couple source, CLVD source, tensile crack source. These radiation patterns provide an intuitive means for interpreting features contained in the data. For example, the s-wave radiation pattern for the double couple source in figure 6(f) clearly shows the polarity reversal pattern seen in the data. Additionally, the amplitudes of the s-wave towards near offset are stronger, which manifests in the radiation pattern as larger lobes. Similar insights can be gained through analysis of the other radiation patterns with comparisons to features in the data.

It is significant to note that these radiation patterns differ greatly from their displace-

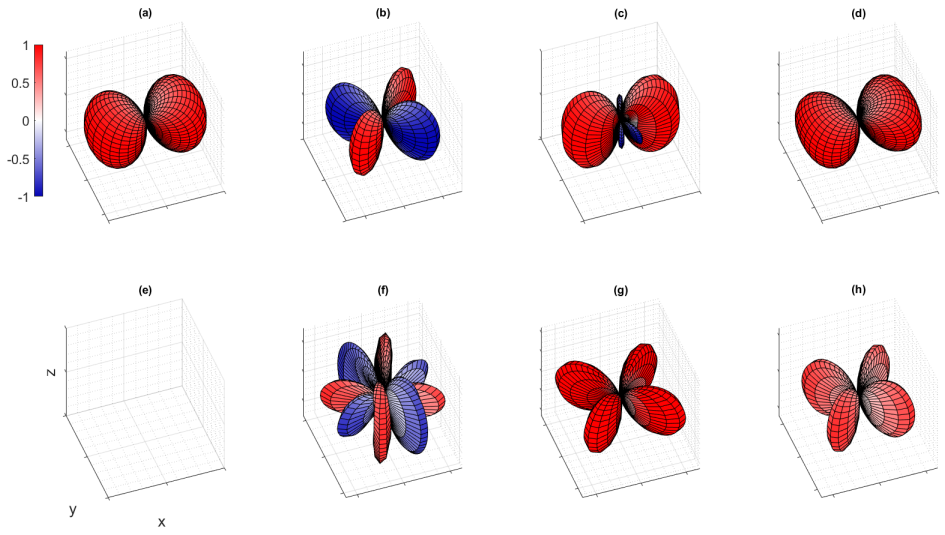

FIG. 6. The ϵ_{xx} compontnet of the p-wave radiation patterns (top row) and s-wave radiation patterns (bottom row) for (a) and (e) explosive source, (b) and (f) double couple source, (c) and (g) CLVD source, and (d) and (h) tensile crack source.

ment counterparts. Using geophones and DAS together may provide complementary datasets that could aid in the interpretation of microseismic datasets and the inversion of moment tensor sources. Shaping fibres increases the tangents they sample and therefore their sensitivity to more of the strain field. In this case the p-wave radiation patterns for a double couple source are a weighted sum of the radiation patterns in figure 4, with the weights supplied by the tangents.

CONCLUSIONS

In this study we present a means of analytically computing the seismic records supplied by a DAS fibre from the waves radiated by microseismic moment tensor sources. Expanding on the work of Aki and Richards (1980) we develop an efficient algorithm for modeling the response of a fibre to many moment tensor sources. Using the geometry of a straight fibre in a horizontal well, we examined the records from four moment tensor sources, which contained features diagnostic of the type of moment tensor source generating the data. In the examples presented here, these diagnostic features can be used to differentiate and characterize the particular source mechanisms generating the data. These examples are fairly simple, and only examined rock failure on planes parallel and perpendicular to the well bore, which is the common direction of failure in hydraulic fracturing. Further analysis should investigate the role of the failure planes on the features seen in the data. Radiation pattern analysis provides an intuitive means for understanding the features seen in the data, and linking them to particular failure mechanism. It is encouraging that the radiation patterns can be used to gain insight into the source mechanics and encourages the use of DAS in conjunction with geophone data to improve the characterization of source mechanisms.

FUTURE WORK

Future work will focus on the investigation of DAS data generated by rock failure on planes that are oblique to the azimuth of the horizontal well. It is possible that the diagnostic features change when this condition is met. It is also of interest to develop strategies for the moment tensor inversion of the data supplied by DAS fibres. At the time of writing the authors are unaware of a method for moment tensor inversion of DAS strain data.

ACKNOWLEDGMENTS

The authors would like to thank the sponsors of the CREWES project as well NSERC under the grant CRDPJ 461179-13 for making this work possible through their financial support. Matt Eaid was partially supported through scholarships from the SEG foundation.

REFERENCES

Aki, K., and Richards, P., 1980, Quantitative Seismology: University Science Books.

Becker, M. W., Ciervo, C., Coleman, T., and Mondanos, M., 2018, Fracture hydromechanical response measured by distributed acoustic sensing at millihertz frequencies: Geophysical Research Letters, **44**, No. 14, 7295–7302.

Cova, R., Hardeman-Vooys, H., Li, D., and McDonald, M., 2018, DAS appliactions for near-surface characterization and traffic conditions assessment: CREWES Research Reports, **30**, No. 7.

Dou, S., Lindsey, N., Wagner, A., Daley, T., Freifeld, B., Robertson, M., Peterson, J., Ulrich, C., Martin, E., and Ajo-Franklin, J., 2017, Distributed acoustic sensing for seismic monitoring of the near surface: A traffic-noise interferometry case study: Scientific Reports, **7**, No. 11620.

Eaid, M., Keating, S., and Innanen, K., 2019, Constructing meaningful FWI gradients for data from shaped DAS fibres: CREWES Research Reports, **31**, No. 12.

Eaid, M., Li, J., and Innanen, K., 2018, Modeling the response of shaped das fibres to microseismic moment tensor sources: SEG Expanded Abstracts.

Innanen, K., 2017, Determination of seismic tensor strain from HWC-DAS cable with arbitrary and nested-helix winds: SEG Expanded Abstracts.

Jin, G., and Roy, B., 2017, Hydraulic-fracture geometry characterization using low-freqeuncy das signal: The Leading Edge, **36**.

Karrenbach, M., and Cole, S., 2019, DAS microseismic source mechanism estimation by forward-modeling: Society for Exploration Geophysicists 89th Annual Meeting, 1004–1008.

Knopoff, L., and Randall, M., 1970, The compensated linear-vector dipole: a possible mechanim for deep earthquakes: Journal of Geophysical Research, **75**, 4957–4963.

Kuvshinov, B. N., 2015, Interaction of helically wound fibre-optic cables with plane seismic waves: Geophysical Prospecting, **64**, No. 3.

Maruyama, T., 1963, On the force equivalents of dynamic elastic dislocations with reference to earthquake mechanism: Bulletin of the Earthquake Research Insitute, Tokyo, **41**, 467–486.

Masoudi, A., Belal, M., and Newson, T., 2013, A distributed optical fibre dynamic strain sensor based on phase-OTDR: Measurement Science and Technology, **24**.

Mateeva, A., Lopez, J., Potters, H., Mestayer, J., Cox, B., Kiyaschenko, D., Wills, P., Grandi, S., K, H., Kuvshinov, B., Berlang, W., Yang, Z., and Detomo, R., 2014, Distributed acoustic sensing for reservoir monitoring with vertical seismic profiling: Geophysical Prospecting, **62**, No. 4, 679–692.

Mestayer, J., Karam, S., Cox, B., Wills, P., Mateeva, A., Lopez, J., Hill, D., and Lewis, A., 2012, Distributed acoustic sensing for geophysical monitoring: 74th EAGE Conference and Exhibition.

Podgornova, O., Leaney, S., Zeroug, S., and Liang, L., 2017, On full-waveform modeling and inversion of fiber-optic VSP data: SEG Expanded Abstracts.